Chem Biol Drug Des 2011; **78:** 787–799

Research Article

doi: 10.1111/j.1747-0285.2011.01187.x

Design, Synthesis and Structure of Novel *Para*-Quinones and their Antibacterial Activity

Komala Pandurangan, Kevin D. Murnaghan, Aurora Walshe, Helge Müller-Bunz, Francesca Paradisi and Grace G. Morgan*

Centre for Synthesis and Chemical Biology (CSCB), School of Chemistry and Chemical Biology, University College Dublin, Belfield, Dublin 4, Ireland
**Corresponding author: Grace G. Morgan, grace.morgan@ucd.ie*

Eight new *para*-quinones and one known analogue have been synthesized from *p*-chloranil. Five have been structurally characterized by single crystal diffraction, and a range of ligand folding is observed. All nine have been tested for their potency towards Gram(+) *S. aureus* and Gram(−) *E. coli*. Quinones 3, 6, 7 and 8 have shown activity towards *S. aureus* and quinones 3 and 8 also show good activity towards *E. coli*.

Key words: antibacterial, crystal structure, *Escherichia coli*, *para*-quinone, *Staphylococcus aureus*

Received 1 February 2011, revised 7 June 2011 and accepted for publication 9 July 2011

It is well known that quinones possess a remarkable range of biological activity. They are essential for many cellular processes including respiration and photosynthesis (1), and there are many naturally occurring quinones that possess antioxidant (2), antiinflammatory (3) and antitumour properties (4,5). They have the ability to act as toxic metabolites and are therefore potentially effective anticancer drugs (6). They have long been cited as having a major role in cellular defence because of their potency in inhibiting bacteria (7), fungi (8) and parasites (9,10).

Para-quinones such as vitamin K derivatives, ubiquinone or plastoquinones play a vital role in energy conversion (photosynthesis and respiration) and information transfer (11–14). Doxorubicin (15) and mitomycin C (16) serve as modern arsenal chemotherapeutic quinones. A variety of *para*-quinone molecules such as Lapachol (17), pixantrone and mitoxantrone are used as chemotherapeutic drugs for cancer treatment. Cytotoxic quinones are postulated to form site-specific free radicals that bind to DNA by intercalation and cross-linking, thereby killing the cancer cells and halting the growth of the tumour (18). The planar structure of quinones enables intercalation with DNA, and the free radical nature of the bound quinone may induce single or double strand breaks in the DNA of carcinoma cells (18). Many quinones exhibit good lipid solubility, and their low hydrophilicity may facilitate penetration of the blood brain barrier making them potentially effective against tumours of the central nervous system (19). The *para*-quinonoid moiety of quinones is an important factor in determining their activity against microorganisms that cause food poisoning and rheumatic fever (20).

Because of this extensive biological activity, design and synthesis of new quinones continues apace (21,22). Amino-substituted *p*-benzoquinones have been shown to have good inhibitory activity towards human colon adenocarcinoma (23) and towards Gram(+) and Gram(−) bacteria (24,25). This led to our interest in preparing and testing a range of new *para*-quinone analogues with the potentially biologically active quinonoid structure (20). The inexpensive starting material *p*-chloranil was used in the attempted synthesis of a range of quinones by reaction with amines I–X, Scheme 1, and the activity of the resulting quinones towards Gram(+) *S. aureus* and Gram(−) *E. coli* was assessed. In this work, nine quinones were successfully prepared by substitution of chloranil of which five were structurally characterized by single crystal diffraction. All were tested for their activity towards Gram(+) *S. aureus* and Gram(−) *E. coli* using the Kirby–Bauer disc-diffusion method (26) and a range of responses was observed.

Experimental Section

General comments

Melting points were determined using a Stuart melting point apparatus (SMP11). Precoated Merck SILICA GEL 60F-254 plates were used for thin layer chromatography, and the spots were detected under UV light (254 nm). Column chromatography was performed using silica gel (0.063–0.200 mm), and the glass column was slurry-packed under gravity. ^{1}H NMR and ^{13}C NMR spectra were recorded on a 300, 400 or 500 MHz Varian spectrometer. The samples were dissolved in DMSO-d_6 or $CDCl_3$, and spectra were recorded in a 5-mm NMR tube. Chemical shifts are reported relative to tetramethylsilane, and coupling constants are given in Hertz. The elemental analysis for C, H and N was performed on an Exeter analytical CE-450 Elemental analyzer. IR spectra were recorded with a Perkin–Elmer Paragon 1000 FT-IR Spectrometer as KBr discs. UV/Vis spectra were recorded with a Unicam UV4 Spectrometer. Electrospray mass spectrometry (MS) was performed with a Perkin Elmer (Waltham, MA, USA) or Waters Micromass (Milford, MA, USA) quadrupole tandem mass spectrometer, using solutions made up in 50% acetonitrile and 50% methanol. MS spectra were obtained in the ES^{+} (electrospray positive ionization) mode for all compounds.

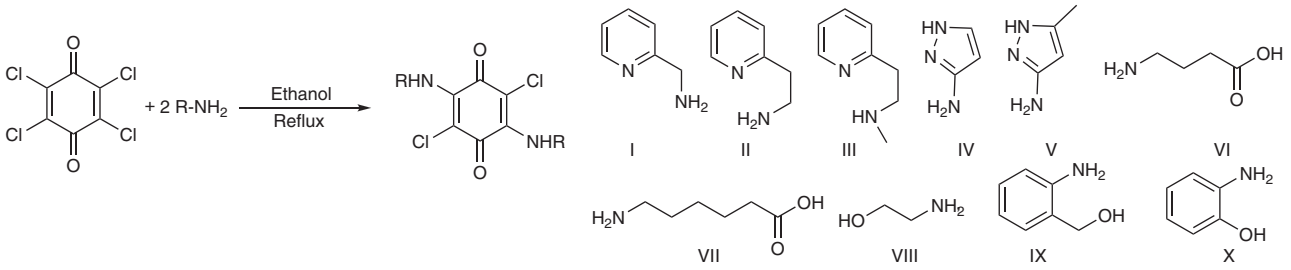

Scheme 1: Synthesis of *p*-quinone analogues from chloranil.

Synthetic procedure

To a well-stirred solution of *p*-chloranil (4.06 mmol) in ethanol (50 mL) was added the neat primary amine (8.12 mmol), and the solution or suspension was heated under reflux at 90 °C for 4–16 h (Table 1). The reaction mixture was cooled to room temperature and filtered. Various coloured products were isolated after recrystallization of the filtered solids, in good yields (Table 1).

2,5-Dichloro-3,6-bis(pyridin-2-ylmethylamino)cyclohexa-2,5-diene-1,4-dione **1**: Yield – 1.50 g (94%). Red-coloured crystals (crystallized from hot acetonitrile). Anal.: calcd. for $C_{18}H_{14}Cl_2N_4O_2$: C, 55.54; H, 3.63; N, 14.39. Found: C, 55.19; H, 3.62; N, 14.22. ESI: 389 (M^+). IR (KBr, /cm), 3193, 3068, 2923, 2361(d), 1660, 1583(d), 1480, 1433(d), 1351, 1320, 1080, 996, 757 and 568.

2,5-Dichloro-3,6-bis(2-(pyridin-2-yl)ethylamino)cyclohexa-2,5-diene-1,4-dione **2**: Yield – 1.40 g (83%). Pink crystals (crystallized from hot acetonitrile). Anal.: calcd. for $C_{20}H_{18}Cl_2N_4O_2$: C, 57.57; H, 4.50; N, 13.43. Found: C, 57.35; H, 4.36; N, 13.24. ESI: 417 (M^+). IR (KBr, /cm), 3109, 2965, 2361(d) 1658, 1578(d), 1498, 1437, 1322, 1219, 1063, 776 and 573.

2,5-Dichloro-3,6-bis(methyl(2-(pyridin-2-yl)ethyl)amino)cyclohexa-2,5-diene-1,4-dione **3**: Yield – 1.55 g (85%). The reaction mixture was filtered and a purple-coloured powder was recovered which on recrystallization from ethanol yielded purple-coloured crystals. UV/vis (CH_3CN): λ_{max}/nm (ε/dm^3 mol^{-1} cm^{-1}) = 259 (3372), 303 (1736). Anal.: calcd. for $C_{22}H_{22}N_4O_2Cl_2$: C, 59.32; H, 4.98; N, 13.43. Found: C, 59.25; H, 4.96; N, 13.10. ESI: 447 (M^+). IR (KBr, /cm): 3271, 3060, 2923, 2850, 1707, 1647 and 990.

2,5-Bis(1H-pyrazol-3-ylamino)-3,6-dichlorocyclohexa-2,5-diene-1,4-dione **4**: Yield – 1.12 g (80%). The green powder on recrystallization in DMF yielded an amorphous green-coloured powder. UV/vis (CH_3CN): λ_{max}/nm (ε/dm^3 mol^{-1} cm^{-1}) = 237 (5870), 357 (4302). Anal.: calcd. for $C_{12}H_8Cl_2N_6O_2$: C, 42.50; H, 2.38; N, 24.78. Found: C, 42.06; H, 2.43; N, 24.05. ESI: 339 (M^+). IR (KBr, /cm), 3312, 3138, 2360(d), 1661, 1573, 1522, 1428, 1320, 1220, 1094, 1005, 861, 671(d) and 590. ^{1}H NMR (400MHz, DMSO- d_6) 12.6 (s, 2H, NH-1Py), 9.3 (s, 2H, NH-2), 7.64 (s, 2H, CH) and 6.10 (d, J = 2.3Hz, 2H). ^{13}CNMR (100MHz, DMSO- d_6) 173.8, 146.1, 144.3, 129.6, 104.3 and 102.57.

2,5-Dichloro-3,6-bis(5-methyl-1H-pyrazol-3-ylamino)cyclohexa-2,5-diene-1,4-dione **5**: Yield – 1.27 g (85%). The green powder on recrystallization in DMF yielded green micro crystals. UV/vis (CH_3CN): λ_{max}/nm (ε/dm^3 mol^{-1} cm^{-1}) = 237 (2637), 285 (1000), 362 (1782). Anal.: calcd. for $C_{14}H_{12}Cl_2N_6O_2$: C, 45.79; H, 3.29; N, 22.89. Found: C, 45.98; H, 3.39; N, 22.49. ESI: 368 (M^+). IR (KBr, /cm), 3400, 3262, 1655, 1577(d), 1514, 1440, 1312, 1222, 1007, 867, 796 and 604. ^{1}H NMR (400 MHz, DMSO- d_6) 12.3 (s, 2H, NH-1Py), 9.25 (s, 2H, NH-2), 5.85 (s, 2H, CH) and 2.19 (s, 6H). ^{13}C NMR (100 MHz, DMSO- d_6) 173.8, 146.2, 144.2, 139.0, 104.1, 101.5 and 11.1.

Diethyl 4,4′-(2,5-dichloro-3,6-dioxocyclohexa-1,4-diene-1,4-diyl)bis(azanediyl)dibutanoate **6**: Yield – 1.15 g (65%). The reddish purple powder on recrystallization in hot acetone yielded purple-coloured crystals. UV/vis (CH_3CN): λ_{max}/nm (ε/dm^3 mol^{-1} cm^{-1}) = 225 (5559), 354 (6793). Anal.: calcd. for $C_{18}H_{24}Cl_2N_2O_6$: C, 49.67; H, 5.56; N, 6.44. Found: C, 49.59; H, 5.41; N, 6.34. ESI: 379 (M^+). ^{1}H NMR (500 MHz, $CDCl_3$) 7.20 (br.s, 2H, NH-), 4.15 (q, 2H, J = 7.1 Hz), 3.92 (q, 6.9 Hz, 2H) 2.41 (t, J = 7.2 Hz, 2H), 2.02 (p, J = 7.2 Hz, 2H) 1.27 (t, J = 7.1 Hz, 3H). ^{13}C NMR (125MHz, $CDCl_3$) δ 172.96, 172.60, 172.33 145.10 (s), 60.70 (s), 43.92 (s), 30.88 (s), 26.00 (s) and 14.17

Table 1: Yields and reaction conditions used in preparation of **1**–**9**

Entry	Primary amine	Conditions[a]	Colour	Yield %
1	2.0 equiv.	Ethanol (50 mL), reflux, 90 °C, 4 h	Red	95
2	2.0 equiv.	Ethanol (50 mL), reflux, 90 °C, 4 h	Dark pink	95
3	2.0 equiv.	Ethanol (50 mL), RT, 90 °C, 4 h	Dark purple	85
4	2.0 equiv.	Ethanol (50 mL), reflux, 90 °C, 4 h	Green	80
5	2.0 equiv.	Ethanol (50 mL), reflux, 90 °C, 4 h	Green	85
6	2.0 equiv.	Ethanol (50 mL), reflux, 90 °C, 16 h	Brown	65
7	2.0 equiv.	Ethanol (50 mL), reflux, 90 °C, 16 h	Metallic brown	70
8[b]	2.0 equiv.	Ethanol (50 mL), 90 °C, 4 h	Purple	90
9	2.0 equiv.	Ethanol (50 mL), reflux, 90 °C, 4 h	Dark green	98

[a]Conventional heating was performed in a thermally preheated oil bath under identical conditions.
[b]Previously reported route employed THF as solvent (28).

(s). IR (KBr, ⁄cm): 3440, 3254(d), 2989, 2369(d), 1723(d), 1581(d), 1200, 1434(d), 1336(d), 1280, 1190, 1074(d) and 580.

Diethyl 6,6′-(2,5-dichloro-3,6-dioxocyclohexa-1,4-diene-1,4-diyl)bis(azanediyl)dihexanoate **7**: Yield – 1.40 g (70%). The hot reaction mixture was filtered, and a purple-coloured product was obtained after evaporation of solvent. The product was purified by column chromatography using pentane⁄chloroform, and the product was isolated as brown-coloured fibrous needles. The reddish brown powder on recrystallization in hot acetone yielded purple-coloured fibres. UV⁄vis (CH_3CN): λ_{max}⁄nm (ε⁄dm^3 mol^{-1} cm^{-1}) = 224 (5644), 355 (6820). Anal.:calcd. for $C_{22}H_{32}Cl_2N_2O_6$: C, 53.77; H, 6.56; N, 5.70%. Found: C, 53.50; H, 6.42; N, 5.71. ^{1}H NMR (500 MHz, $CDCl_3$) 7.13 (br.s, 2H, NH-), 4.13 (q, *J* = 7.1 Hz, 2H), 3.88 (dd, *J* = 14.2, 6.9 Hz, 2H), 2.33 (dd, *J* = 15.6 Hz, J = 8.1Hz 2H), 1.76–1.57 (m, 2H), 1.49–1.34 (m, 2H), 1.26 (t, *J* = 7.1 Hz, 3H. ^{13}C NMR (125 MHz, $CDCl_3$) δ 173.76, 173.33, 172.22, 145.80, 60.29, 44.58, 33.93, 30.53, 26.02, 24.41 and 14.21. ESI: 439 (M^+). IR (KBr, ⁄cm) -3421, 3100, 2940, 2858, 1737, 1567, 1489, 1369, 1337, 1162, 1069, 792 and 580.

2,5-Dichloro-3,6-bis(2-hydroxyethylamino)cyclohexa-2,5-diene-1,4-dione **8**: Yield – 1.08 g (90%). The purple-coloured product was obtained after evaporation of solvent. The purple powder on recrystallization in hot ethanol yielded purple-coloured crystals. UV⁄vis (CH_3CN): λ_{max}⁄nm (ε⁄dm^3 mol^{-1} cm^{-1}) = 226 (1202), 290 (681), 357 (385). Anal.: calcd. for $C_{10}H_{12}Cl_2N_2O_4$: C, 40.70; H, 4.10; N, 9.49. Found: 40.42; H, 3.9; N, 9.26. ESI: 295 (M^+). IR (KBr, ⁄cm): 3423(s), 3195(s), 2360(d), 1578(d), 1500(s), 1447, 1333, 1296, 1212, 1035 and 786. ^{1}H NMR (400MHz, DMSO- d_6) 7.84 (s, 2H), 4.95 (br.s, 2H), 3.8(q, *J* = 5.9 Hz, 4H) and 3.56 (t, 4H). ^{13}C NMR (100 MHz, DMSO-d_6) δ 171.77, 145.95, 98.71, 60.52 and 46.68.

2,5-Dichloro-3,6-bis(2-(hydroxymethyl)phenylamino)cyclohexa-2,5-diene-1,4-dione **9**: Yield – 1.66 g (98%). Dark green crystals (recrystallized from ethanol). UV⁄vis (CH_3CN): λ_{max}⁄nm (ε⁄dm^3 mol^{-1} cm^{-1}) = 270 (3214), 387 (2629). Anal.: calcd. for $C_{20}H_{16}C_{l2}N_2O4$: C, 57.30; H, 3.85; N, 6.68. Found C, 57.30; H, 3.75; N, 6.80. ESI: 419 (M^+). IR (KBr, ⁄cm): 3465, 3213 2360 (d), 1605, 1567 (d), 1501, 1469 (d), 1327, 1186 (d), 893, 753 and 576. ^{1}H NMR (400 MHz, DMSO-d_6) 9.45 (s, 2H), 7.38 (dd, 1H, *J* = 7.1, 1.9 Hz), 7.24 (pd, *J* = 7.4, 1.7 and 2.8 Hz), 7.08 (dd, *J* = 8.9, 7.1 Hz), 5.38 (s, 1H) and 4.68 (s, 2H). ^{13}C NMR (100 MHz, DMSO-d_6) 172.2, 142.1, 135.5, 134.6, 125.9, 125.27, 125.04, 101.8 and 59.3.

Antibacterial studies

The antibacterial activity of **1**–**9** was screened against two bacterial strains: Gram(+) *Staphylococcus aureus* (NCTC 7447) and Gram(–) *Escherichia coli*. To assess the biological activity of compounds **1**–**9**, the Kirby–Bauer disc-diffusion method was applied (26). All bacteria were individually cultured from a single colony in a sterile LB medium (27) overnight at 37 °C (orbital shaker incubator). All the work was performed under sterile conditions.

For each strain, 70 μL of culture were spread evenly on an agar-LB medium. Four 5-mm diameter paper discs were placed evenly separated on each plate. Stock solutions (DMSO) of all the compounds were prepared by dissolving 10 mg in 100 μL to test the effect in different concentrations. Each plate was then tested with 3, 6, 9 and 12 μL of stock solution. The plates were covered and placed in an incubator at 37 °C for 24 h. The plates were then removed, and the zone of clearance (defined as the diameter of inhibited bacterial growth around the filter paper) for each sample was measured in millimetres.

Results and Discussion

Synthesis

Synthesis of ten new quinones (**1–7** and **9**, Table 2) and one known example, compound **8** (28), was attempted, by refluxing the appropriate amine with *p*-chloranil in ethanol, Scheme 1, of which nine (**1–9**) were successful. Compound **10** did not form, instead the starting amine, 2-aminophenol (X), was observed to dimerise in the presence of *p*-chloranil to produce 2-aminophenoxazine-3-one. Our results on the antibacterial activity of the resulting 2-aminophenoxazine-3-one and its silver(I) complex are reported elsewhere (29). The two carboxylic acids VI and VII reacted with the ethanol solvent to produce the ethyl esters, **6** and **7**, Table 2. Formation of the di-esters **6** and **7** is confirmed by NMR, IR, elemental analysis and by a crystal structure of **6**. Formation of di-esters rather than the free acid has been previously observed for several amino acids (30,31). Addition of the primary amine to the *p*-chloranil produced intensely coloured solutions that were filtered after 4 h. In the case of amines I, II, IV, V and IX, highly coloured powders of products **1**, **2**, **4**, **5** and **9** precipitated immediately and were collected by suction filtration and recrystallized from acetone or hot acetonitrile yielding X-ray quality crystals of **1**, **2**, **6** and **9** (Table 1). Quinones **3**, **6**, **7** and **8** were recovered as powders that were purified by column chromatography. The resulting precipitates were recrystallized from various solvents that yielded X-ray quality crystals in the case of product **3**.

Characterization

The synthesized quinones were characterized by ^{1}H NMR, ^{13}C NMR, elemental analysis and mass spectrometry (see Experimental section). Compounds **4, 5, 6, 7, 8** and **9** have a characteristic ^{1}H NMR signal at around 7.2–7.35 p.p.m. for the NH proton on the amine attached to the quinone ring and **4** and **5** also have a pyrazole ring NH signal at *ca.* 9.4–9.1 p.p.m.. The ^{13}C NMR spectra typically have aromatic signals at 100–150 p.p.m. and a resonance at *ca.* 170 p.p.m. for the carbonyl carbon of the *p*-quinone core. Full assignment of the ^{13}C and ^{1}H NMR spectra is given in the Experimental section. For compounds **1** and **2,** ^{1}H NMR and ^{13}C NMR were not recorded because of the poor solubility of the compounds in routine solvents including chloroform, methanol and DMSO. However, it was possible to grow single crystals of these compounds from hot acetonitrile, and their solid state structures have been determined by single crystal diffraction. IR spectroscopic stretching frequencies for **1**–**9** have characteristic absorptions between 1600 and 1550⁄cm for the quinone carbonyl group and between 3000 and 3200⁄cm for the NH group. In addition, compounds **6** and **7** have a characteristic stretching frequency for

Table 2: *In vitro* antibacterial activity of *p*-quinones **1–9**

Compound		MIC (μmol/mL)	Diameter of clearance (mm)	
			SA	EC
1	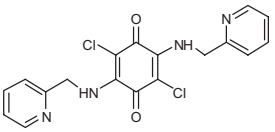	–	NS	NS
2	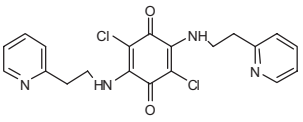	–	NS	NS
3	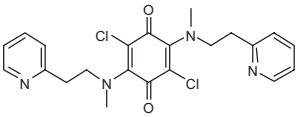	2.72	14	12
4	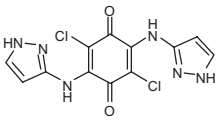	–	NA	NA
5	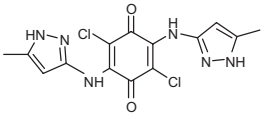	–	NA	NA
6	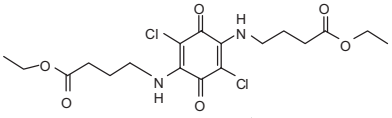	3.16	9	NA
7	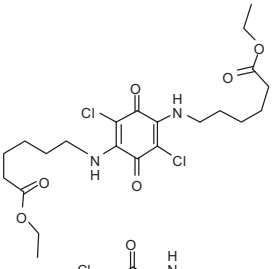	2.76	9	NA
8	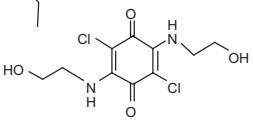	4.08	6	8
9	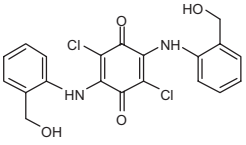	–	NA	NA

NS, not soluble; NA, no activity; SA, *S. aureus*; EC, *E. coli*; MIC, minimum inhibitory concentration of the sample used. The assay was performed at 37 °C. Both bacteria were individually cultured from a single colony in LB medium.

the ester carbonyl at 1723/cm, and compounds **8** and **9** have a characteristic peak at 3200–3470/cm for the alcohol OH group, Table 3. Elemental analysis of all the compounds is in close agreement with the calculated values, and mass spectrometry shows the parent molecular weight in all cases. Electronic absorption spectra of **1–9**, Table 3, typically have λ_{max} around 300–390 nm, which is characteristic for *p*-benzoquinones (24). Compounds **6** and **7** also have a band at 354 nm characteristic of the ester group (30,31). In addition to these, data compounds **1, 2, 3, 6** and **9** were structurally characterized by single crystal diffraction.

Table 3: Characterization data of **1–9**

Entry	^{13}C NMR (d_6-DMSO) (^{1}H NMR data in experimental)	Characteristic IR[c] frequencies in per cm	λ_{max} (nm)[d]	Melting point (°C)
1[a]	–	3193, 3068, 2923, 2361(d), 1660, 1583(d), 1480, 1433(d), 1351, 1320, 1080, 996, 757 and 568	–	154–156
2[a]	–	3109, 2965, 2361(d) 1658, 1578(d), 1498, 1437, 1322, 1219, 1063, 776 and 573	–	183–185
3	Not measured	3271, 3060, 2923, 2850, 1707, 1647 and 990	259, 303	144–145.5
4	173.8, 162.7, 146.1, 144.3, 129.6, 104.3 and 102.5	3312, 3138, 2360 (d), 1661, 1573, 1522, 1428, 1320, 1220, 1094, 1005, 861, 671 (d) and 590	237, 357	Above 280
5	173.8, 146.2, 144.2, 139.0, 104.1, 101.5 and 11.1.	3400, 3262, 1655, 1577(d), 1514, 1440, 1312, 1222, 1007, 867, 796 and 604	231, 285, 362	Above 280
6[b]	172.9, 172.6, 172.3, 145.1 (s), 60.7 (s), 43.9 (s), 30.9 (s), 26.0 (s) and 14.1 (s).	3440, 3254(d), 2989, 2369(d), 1723(d), 1581(d), 1200, 1434(d), 1336(d), 1280, 1190, 1074(d) and 580	225, 354	107–108
7[b]	173.8, 173.3, 172.2, 145.8, 60.3, 44.6, 33.9, 30.5, 26.0, 24.4 and 14.2	3421, 3100, 2940, 2858, 1737, 1567, 1489, 1369, 1337, 1162, 1069, 792 and 580	223, 354	116–118
8	171.8, 145.9, 98.7, 60.5 and 46.7	3423(s), 3195(s), 2360(d), 1578(d), 1500(s), 1447, 1333, 1296, 1212, 1035 and 786	226, 290, 357	166–168
9	172.2, 142.1, 135.5, 134.6, 125.9, 125.2, 125.0, 101.8 and 59.3	3465, 3213 2360 (d), 1605, 1567 (d), 1501, 1469 (d), 1327, 1186 (d), 893, 753 and 576	270, 387	206–207

[a]Solution NMR and UV/VIS spectra not recorded because of poor solubility.
[b]$CDCl_3$ solutions.
[c]IR recorded using KBr disc.
[d]Acetonitrile solution at room temperature.

Table 4: Quinone ring bond lengths of **1, 2, 3, 6** and **9**

Entry	Bond	Bond length (Å)				
		1	**2**	**3**	**6**	**9**
1	C1–O1	1.228 (3)	1.231 (3)	1.218 (15)	1.232 (14)	1.231 (2)
2	C1–C2	1.424 (3)	1.422 (4)	1.456 (18)	1.426 (16)	1.423 (2)
3	C2–C3	1.363 (3)	1.367 (4)	1.362 (17)	1.379 (16)	1.370 (2)
4	C2–Cl	1.741 (2)	1.734 (3)	1.731 (12)	1.735 (12)	1.733 (16)
5	C3–NHR	1.323 (3)	1.330 (4)	1.364 (16)	1.329 (15)	1.326 (2)

X-ray crystal structure analysis

Although crystal structure analysis alone is insufficient to predict antibacterial activity, it is an important property of any bioactive molecule, particularly as polymorphism is known to affect solubility and hence biological action. Attempts were therefore made to crystallize all nine quinones reported here and determine their solid state structures. Single crystals of compounds **1, 2, 3, 6** and **9** were grown by slow evaporation at room temperature and their structures determined by single crystal X-ray diffraction at 100 K (with the exception of **3** which was determined at room temperature). Structural parameters are listed in Table 4, and the structures are shown in Figures 1–5. Selected bond lengths including the internal quinone ring and quinone–heteroatom bond length ranges are given in Table 4. Complete bond lengths and angles for all are provided in the Supporting Information.

Analysis of the bond lengths and angles confirms that all exist in the diamagnetic quinone form with regular carbon–oxygen ketonic bond lengths and carbon–nitrogen distances expected for a single bond, Table 4. All five structures have an inversion centre in the middle of the quinone ring, and a striking aspect of the solid state structures is the wide variation in local geometry on changing R.

Structure of 1

Compounds **1–3** contain an appended pyridine group linked to the central quinone by a methylene or ethylene group on a secondary (compounds **1** and **2**) or tertiary (compound **3**) amine on the quinone. The nature of the bridge between the central quinone and peripheral pyridine has a profound effect on the packing. Compound **1**, where the two heterocyclic rings are linked *via* a methylene group, Figure 1A, is almost planar, Figure 1B. The planar molecules pack in a layered structure, Figure 1C, which arises from the stacking of the pyridine and amine nitrogens above two of the quinone ring carbons, Figure 1(D) leading to the undulating sheets.

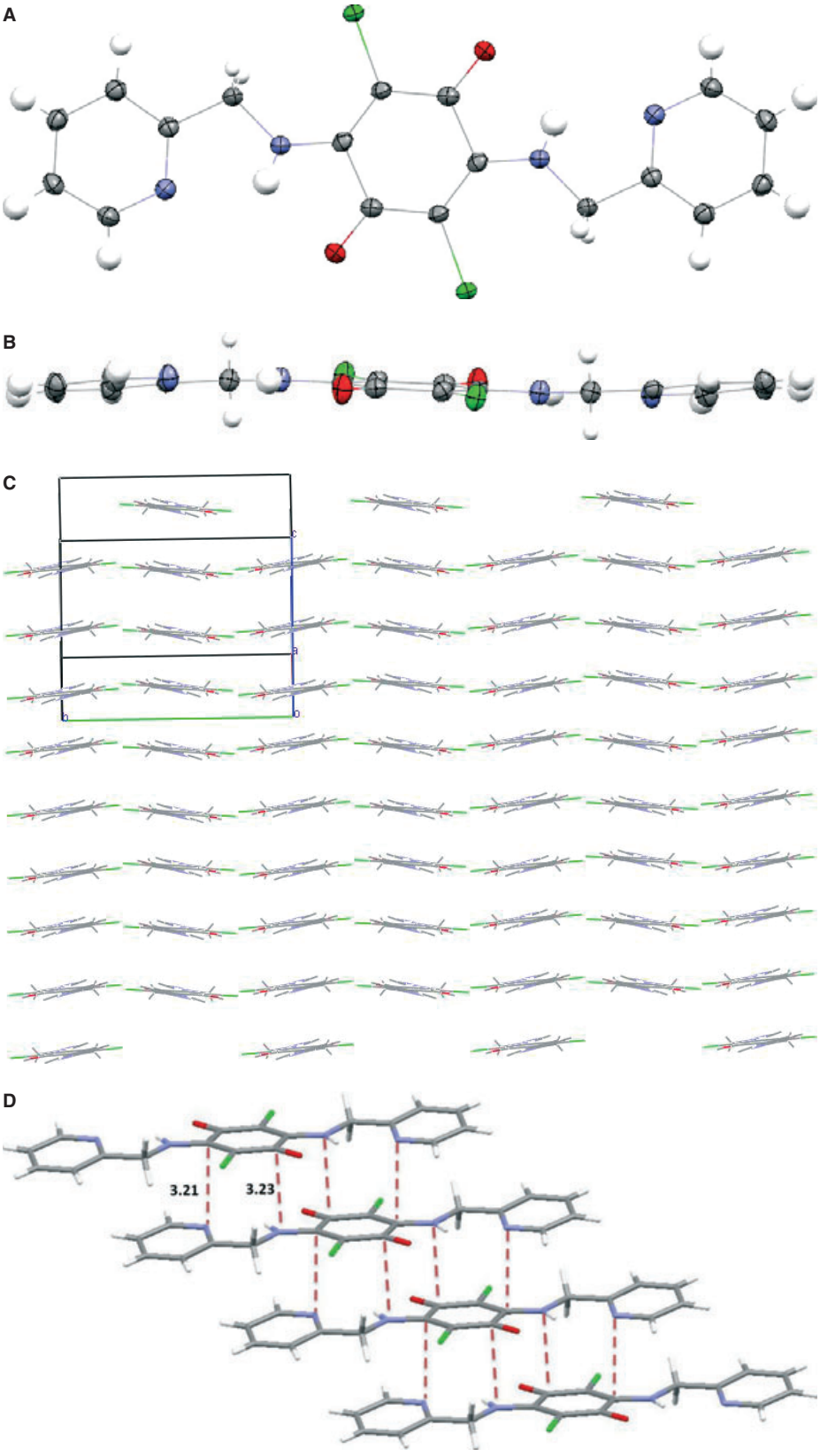

Figure 1: (A) View of compound **1**; (B) side-on view of **1** showing planarity of molecule; (C) packing diagram of **1** showing 2-D layered structure; (D) View of local stacking.

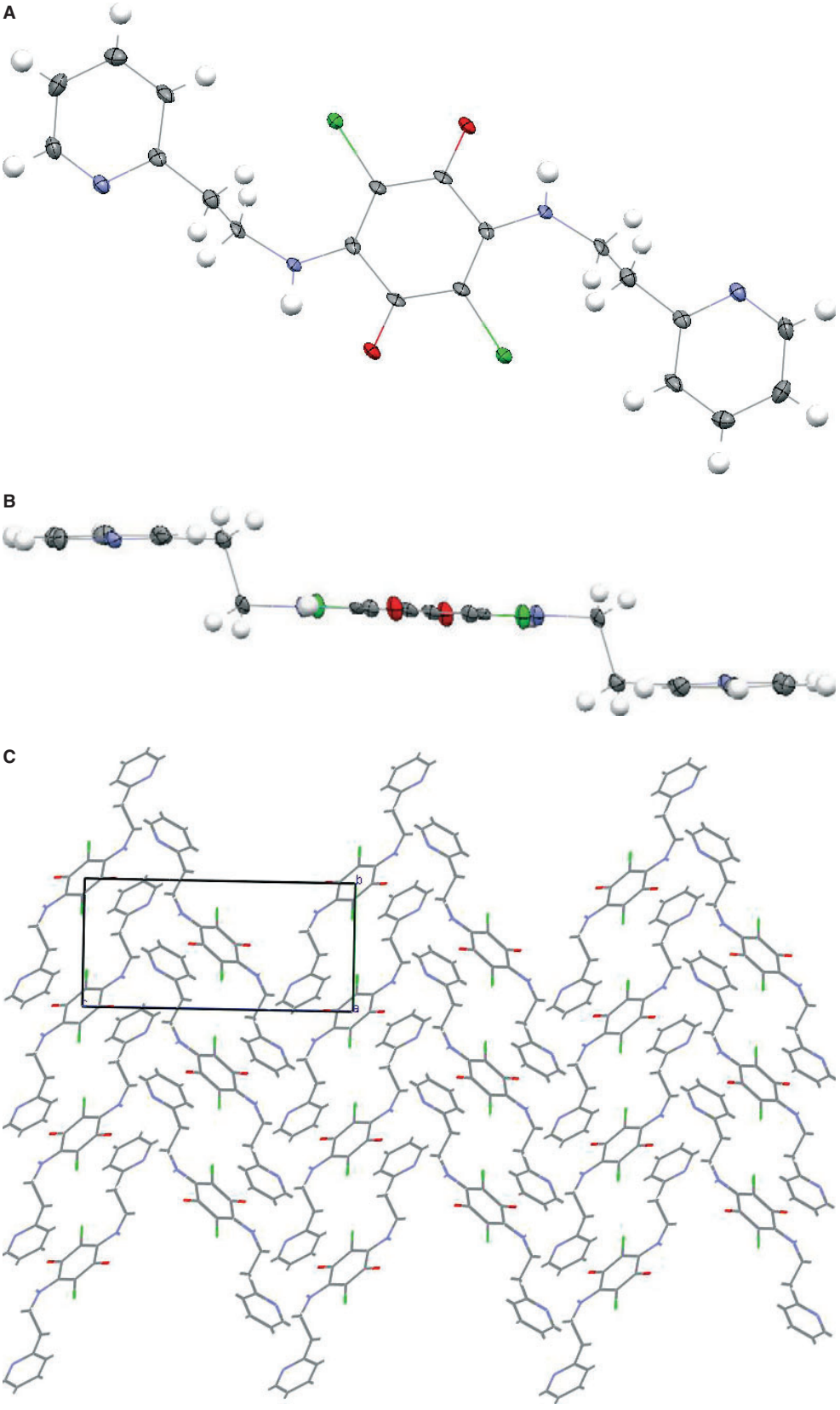

Figure 2: (A) View of compound **2**; (B) side-on view of **2** showing stepped arrangement; (C) packing diagram of **2**.

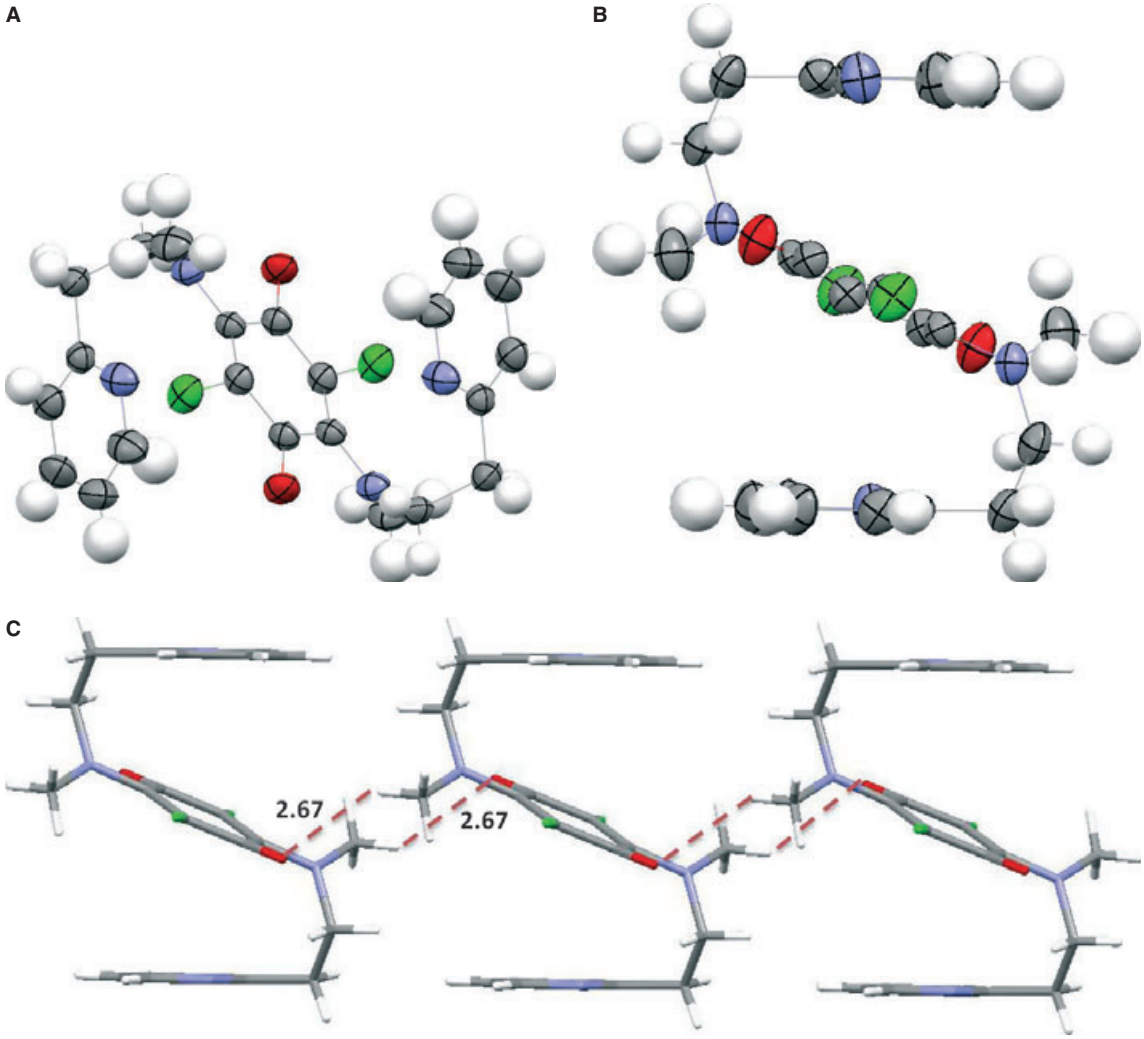

Figure 3: (A) View of compound **3**; (B) side-on view of **3** showing S-shaped arrangement; (C) view of hydrogen bonding in **3**.

Structure of 2

When the methylene linkage is replaced with ethylene in compound **2,** the planarity is lost and the molecule adopts a stepped arrangement, Figures 2A,B. As for compound **1**, both pyridine rings point away from the central quinone. There are no intermolecular interactions, and the packing of the stepped molecule, Figure 2C, is presumably governed solely by packing efficiency.

Structure of 3

Compound **3** is very similar to compound **2**; the only change is that the secondary amine hydrogen has been replaced by a methyl group, but the local geometry is very different, Figure 3A, and the molecule now adopts a distinct S-shape (Figure 3B). Strong intermolecular interactions between the quinone oxygen and the CH_2 group on an adjacent molecule leads to an in-plane ordering of the S-shaped molecules, Figure 3C, and this extends into a 2-D lattice by an interaction between the pyridine nitrogen and a pyridine CH on an adjacent molecule.

The solubility of **3** in DMSO is good in contrast to that of the other two pyridine substituted quinones **1** and **2** and is attributed to the methyl group on the amine. It is interesting to note that **3** is the most active compound in the series suggesting that the combination of pyridine and 1,4-benzoquinone rings is highly effective but the compound must be soluble to be active.

Structure of 6

Compound **6** differs from **1–3** as it has linear ester groups appended, rather than pyridine rings (Figure 4A). The conformation is clearly chair shaped, Figure 4B, and adjacent molecules are linked by a double donor-acceptor hydrogen bonding motif where each quinone oxygen and secondary amine hydrogen on one molecule hydrogen bond to the NH and quinone oxygen on their nearest neighbour, thus keeping the rings in plane (Figure 4C). This leads to an efficient herringbone packing pattern (Figure 4D).

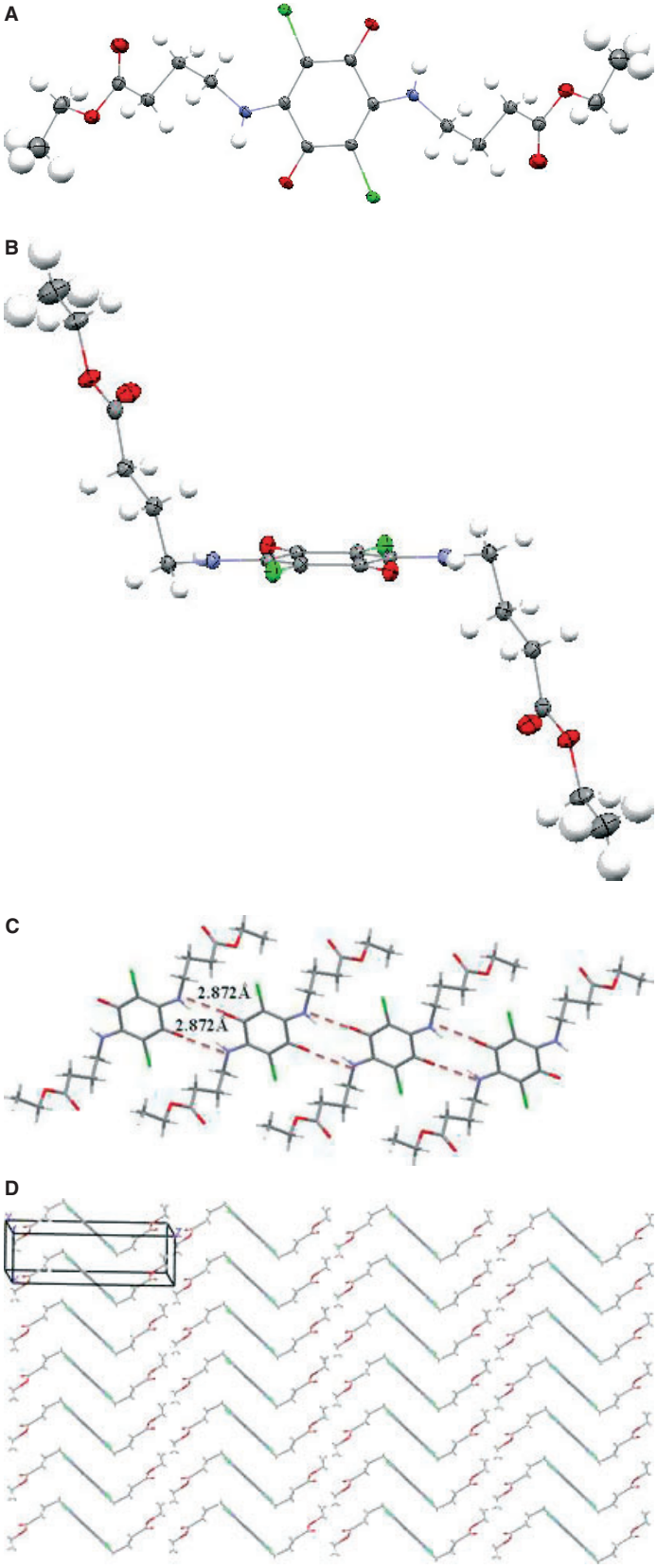

Figure 4: (A) View of compound **6**; (B) side-on view of **6** showing stepped arrangement; (C) hydrogen bonding in **6**; (D) Packing diagram of **6.**

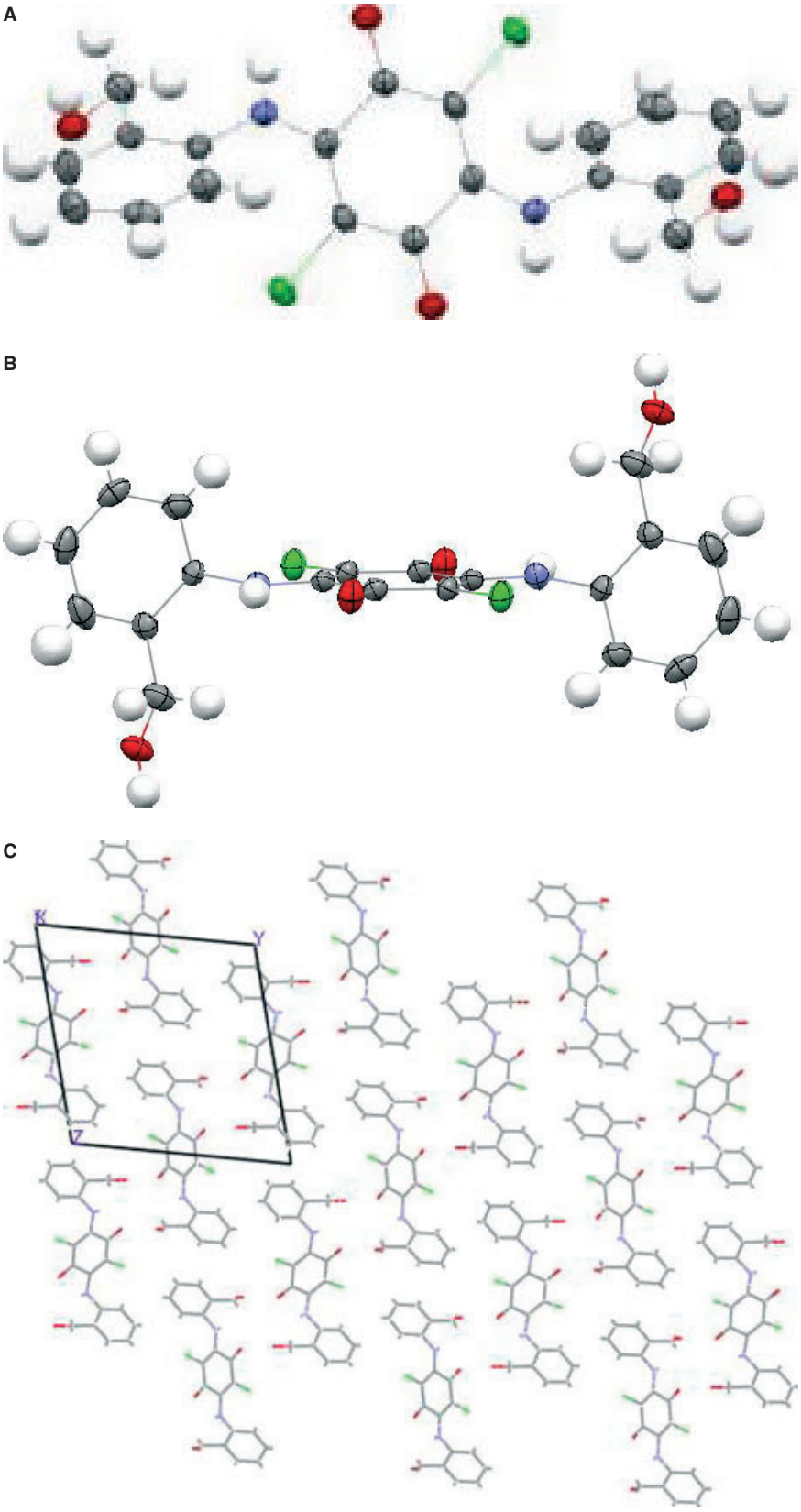

Figure 5: (A) View of compound **9**; (B) side-on view of **9** showing out-of-plane twist of appended rings; (C) packing diagram for **9**.

Structure of 9

Unlike **1–3** and **6**, compound **9** does not contain a spacer between the appended R group and the secondary amine of the quinone, Figure 5A. The appended benzyl alcohol groups both twist out of the plane of the central quinone ring, Figure 5B, presumably to minimize packing energy, and the resulting packing is less efficient than the herringbone pattern of **6**.

Bond lengths of quinones

The C–O distances of 1.21–1.23 Å are in close agreement with those observed for the *p*-quinone compounds (22,32). The C–C bond lengths of 1.36–1.46 Å in the quinone rings are also in close agreement with those observed for the *p*-quinone ligands, as are the C–Cl bond lengths of 1.73–1.74 Å (33,34).

Antibacterial testing

Antibacterial activity of compounds **1–9** towards Gram(+) *S. aureus* and Gram(–) *E. coli* were compared using the Kirby–Bauer disc-diffusion method and results are shown in Table 2. For comparative purposes, compounds **1–9** can be broadly classified according to the nature of the R group. Using this classification, the compounds can be grouped into five N-heterocyclic ligands with pyridine (**1–3**) or pyrazole (**4** and **5**) substituents. The remaining four fall into two categories: two long chain ethoxy esters (**6** and **7**) and two alcohols (**8** and **9**). The activity of all towards *S. aureus* and *E. coli* will be discussed. Pyridine-containing quinones **1** and **2** were measured as solid samples applied as spots on the Petri dishes. All other compounds were loaded as solutions in DMSO.

Activity towards Gram(+) S. aureus

Compounds **1**, **2**, **4**, **5** and **9** were inactive whilst **3**, **6**, **7** and **8** showed varying degrees of activity. Pyridine ligand **3** showed the greatest activity, Figure 6. Therefore, it might be reasonable to expect that the other pyridine ligands **1** and **2** would also be active. The absence of any activity may then be due to solubility differences rather than inherent inactivity as **1** and **2** were the only compounds to be spotted as solid samples. However, this alone does not definitively explain the inactivity as compound 9 was also inactive towards both bacteria despite being applied in solution. In contrast to pyridine ligand **3**, the N-heterocyclic pyrazoles **4** and **5** were totally inactive towards *S. aureus*.

When ester groups are appended, some activity is observable, Figure 6, and **6** and **7** show similar activity to each other but not so much as for pyridine derivative **3**. Finally, the alcohols **8** and **9** show very different activity with no activity for benzyl alcohol derivative **9** in contrast to the good activity of **8** that is the second most active of the set towards *S. aureus*. The major difference between these is the presence of the benzene ring in **9** suggesting that decreasing the polarity reduces the activity.

Activity towards Gram(–) E. coli

The pattern of activity of the N-heterocyclic quinones towards the *E. coli* is the same as for the activity towards *S. aureus*. Compounds **1**, **2**, **4**, **5**, **6**, **7** and **9** were inactive whilst **3** and **8** showed reasonable activity (Figure 7). Again the solubility problems of pyridine ligands **1** and **2** may affect the measurement, so it is not possible to absolutely conclude whether they are inactive or if solid spotting explains the lack of response. In contrast to these, pyridine ligand **3** shows most activity of the whole series **1–9**, as was the case in the *S. aureus* investigation. However, the pyrazole derivatives **4** and **5** are again inactive in the antibacterial test. As was the case for the N-heterocyclic ligands, the activity of the two alcohols **8** and **9** towards *E. coli* mirrors that of their activity towards *S. aureus* in that the ethyl alcohol **8** is observed to be active whilst the benzyl alcohol **9** is inactive. The only functional group to show a difference in the behaviour towards the two bacterial types is the ester, as it is now observed that esters **6** and **7** are inactive towards *E. coli* in contrast to their good activity towards *S. aureus*. The sample solvent (DMSO) was also inactive towards both bacteria as previously reported (35).

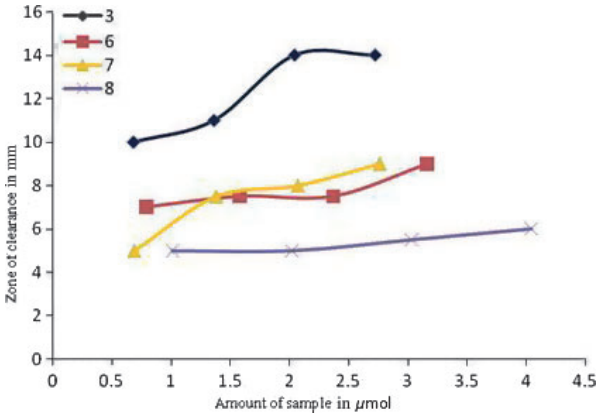

Figure 6: Zone of clearance for active compounds **3**, **6**, **7** and **8** towards Gram(+) *S. aureus*. Inactive compounds **1**, **2**, **4**, **5** and **9** had zero zone of clearance and are not shown.

Given the redox lability of quinones, the antibacterial activity of some members of the series is likely because of their ability to

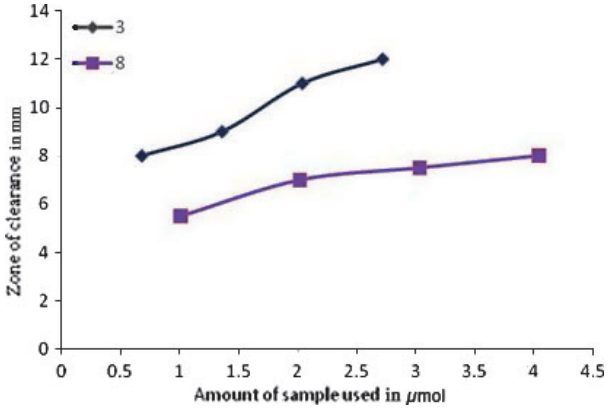

Figure 7: Zone of clearance for active compounds **3** and **8** towards Gram(–) *E. coli*. Inactive compounds **1**, **2**, **4**, **5**, **6**, **7** and **9** had zero zone of clearance and are not shown.

form the toxic semiquinone radical, which is a potent reactive oxygen species (ROS) (36). Production of ROS causes oxidative stress as the radicals react readily with most bio-molecules to initiate a chain reaction of free radical formation that can be terminated only after reaction with another free radical or free radical scavengers such as antioxidants. These ROS can react with all the macromolecular machinery of cells particularly lipids proteins and DNA (36,37). This most probably accounts for the reactivity of certain quinones in the series towards Gram(+) and Gram(–) bacteria. Whilst a significant number of quinones **1–9** showed activity towards *S. aureus,* fewer were active towards *E. coli*, and in general, the activity was not so potent as that observed in a related set of *p*-quinone derivatives where the Kirby–Bauer method was also used to assess antibacterial efficacy (24). In this series, described by Batra *et al.*, a pair of substituted phenyl rings is appended onto the 3-6-dichloro-1,4-benzoquinone core and zonal clearance ranges from 8.5–12.5 mm for *S. aureus* and 8.6–14.1 mm for *E. coli*. In comparison with these values, only compound **3** in our series shows strong activity suggesting that the nature of the appended aromatic group is significant in determining activity.

Conclusion

In our work, we have shown the synthesis of *p*-quinone analogues with different functionalities in good yields. Substitution of analogue **2** with a methyl group yields **3** that exhibits good antibacterial activity. All synthesized quinones have been chemically characterized, and five were characterized by single crystal diffraction. Structural analysis reveals a variety of ligand conformations in the solid state including S-, Z- and planar-arrangements. The S-shaped pyridine substituted quinone **3** was most active and was also the only soluble member of the pyridine quinone set **1–3**. Antimicrobial activity towards Gram(+) and Gram(–) bacteria was assessed showing that some members of the series had good antimicrobial activity. Studies are underway to assess the anticancer activity of these quinones and to synthesize their metal complexes to test these for their antimicrobial activity.

Acknowledgments

The award of a Government of Ireland Postgraduate Scholarship to (K.P.) by the Irish Research Council for Science, Engineering and Technology (IRCSET) is gratefully acknowledged as is the award of an Enterprise Ireland Postgraduate Scholarship to (K.D.M.) Financial support from the UCD School of Chemistry and Chemical Biology is also gratefully acknowledged.

References

1. Bernardo P.H., Chai C.L.L., Guen M.L., Smith G.D., Waring P. (2007) Structure–activity delineation of quinones related to the biologically active Calothrixin B. Bioorg Med Chem Lett;17:82–85.
2. Yen G.-C., Duh P.-D., Chuang D.-Y. (2000) Antioxidant activity of anthraquinones and anthrone. Food Chem;70:437–441.
3. Kuo Y.-C., Meng H.-C., Tsai W.-J. (2001) Regulation of cell proliferation, inflammatory cytokine production and calcium mobilization in primary human T lymphocytes by emodin from *Polygonum hypoleucum Ohwi*. Inflamm Res;50:73–82.
4. Karczewski J.M., Peters J.G.P., Noordhoek J. (1999) Quinone toxicity in DT-diaphorase-efficient and -deficient colon carcinoma cell lines. Biochem Pharmacol;57:27–37.
5. Hazra B., Kumar B., Biswas S., Pandey B.N., Mishra K.P. (2005) Enhancement of the tumour inhibitory activity, in vivo, of diospyrin, a plant-derived quinonoid, through liposomal encapsulation. Toxicol Lett;157:109–117.
6. Lin A.J., Cosby L.A., Sartorelli A.C. (1974) Quinones as anticancer agents: potential bioreductive alkylating agents. Cancer Chemother Rep Part 2;4:23–25
7. Hoover J.R.E., Day A.R. (1954) Preparation of some imidazole derivatives of 1,4-naphthoquinone. J Am Chem Soc;76:4148–4152.
8. Curreli N., Sollai F., Massa L., Comandini O., Rufo A., Sanjust E., Rinaldi A., Rinaldi A.C. (2001) Effects of plant-derived naphthoquinones on the growth of *Pleurotus sajor-caju* and degradation of the compounds by fungal cultures. J Basic Microbiol;41:253–259.
9. Howland J.L. (1963) The reversibility of inhibition by 2-heptyl-4-hydroxyquinoline-n-oxide and 2-hydroxy-3-(3-methylbutyl)-1,4-naphthoquinone of succinate oxidation. Biochim Biophys Acta;73:665–667.
10. Mukerjee P., Majee S.B., Ghosh S., Hazra B. (2009) Apoptosis-like death in *Leishmania donovani* promastigotes induced by diospyrin and its ethanolamine derivative. Int J Antimicrobiol;34:596–601.
11. Izumi Y., Sawada H., Sakka N., Yamamoto N., Kume T., Katsuki H., Shimohama S., Akaike A. (2005) *p*-Quinone mediates 6-hydroxydopamine-induced dopaminergic neuronal death and ferrous iron accelerates the conversion of *p*-quinone into melanin extracellularly. J Neurosci Res;79:849–860.
12. Furie B., Bouchard B.A., Furie B.C. (1999) Vitamin K-dependent biosynthesis of g-carboxyglutamic acid. Blood;93:1798–1808.
13. Meganathan R. (2001) Biosynthesis of menaquinone (vitamin K2) and ubiquinone (coenzyme Q): a perspective on enzymatic mechanisms. Vitam Horm;61:173–218.
14. Sheldon P.J., Shelman D.H. (2001) Characterization of quinone reductase activity for the mitomycin C binding protein (MRD): functional switching from a drug-activating enzyme to a drug-binding protein. Proc Natl Acad Sci U S A;98:926–931.
15. Frederick C.A., Williams L.D., Ughetto G., van der Marel G.A., van Boom J.H., Rich A., Wang A.H.-J. (1990) Structural comparison of anticancer drug-DNA complexes: adriamycin and daunomycin. Biochemistry;29:2538–2549.
16. Begleiter A., Leith M.K., Thliveris J.A., Digby T. (2004) Dietary induction of NQO1 increases the antitumour activity of mitomycin C in human colon tumours in vivo. Br J Cancer;91:1624–1631.
17. Linardi M.C.F., de Oliveira M.M., Sampaio M.R.P.A. (1975) Lapachol derivative active against mouse lymphocytic leukemia P-388. J Med Chem;18:1159–1161.
18. Bachur N.R., Gordon S.L., Gee M.V.A. (1978) General mechanism for microsomal activation of quinone anticancer agents to free radicals. Cancer Res;38:1745–1750.

19. Chou F., Khan A.H., Driscoll J.S. (1976) Potential central nervous system antitumour agents. Aziridinylbenzoquinones. J Med Chem;19:1302–1308.
20. Lana E.J.L., Carazza F., Takahashi J.A. (2006) Antibacterial evaluation of 1,4-benzoquinone derivatives. J Agric Food Chem;54:2053–2056.
21. Ong W., Yang Y., Cruciano A.C., McCarley R.L. (2008) Redox-triggered contents release from liposomes. J Am Chem Soc;130:14739–14744.
22. Nicolaou K.C., Becker J., Lim Y.H., Lemire A., Neubauer T., Montero A. (2009) Total synthesis and biological evaluation of (+)- and (−)-bisanthraquinone antibiotic BE-43472B and related compounds. J Am Chem Soc;131:14812–14826.
23. Mathew A.E., Zee-Cheng R.K.Y., Cheng C.C. (1986) Amino-substituted *p*-benzoquinones. J Med Chem;29:1792–1795.
24. Batra M., Kriplani P., Batra C., Ojha K.G. (2006) An efficient synthesis and biological activity of substituted *p*-benzoquinones. Bioorg Med Chem;14:8519–8526.
25. Batra M., Batra C., Ojha K.G. (2008) Non-traditional approaches to the synthesis of some biologically active substituted *p*-benzoquinones. Med Chem Res;17:604–617.
26. Bondi A., Spaulding H.E., Smith E.D., Dietz C.C. (1947) Routine method for rapid determination of susceptibility to penicillin and other antibiotics. Am J Med Sci;213:221–225.
27. Luria S.E. (1947) Recent advances in bacterial genetics. Bacteriol Rev;11:1–40.
28. Zhang S., Earle J., MacDiarmid J., Bardos T.J. (1988) Synthesis and testing of quinone-based bis(2,2-dimethyl-l-aziridinyl)phosphinyl carbamates as radiation-potentiating antitumor agents. J Med Chem;31:1240–1244.
29. Pandurangan K., Gallagher S., Morgan G.G., Müller-Bunz H., Paradisi F. (2010) Structure and antibacterial activity of the silver(I) complex of 2-aminophenoxazine-3-one. Metallomics;2:530–534.
30. Jones G., Qian X. (1998) Photochemistry of quinone-bridged amino acids. Intramolecular trapping of an excited charge-transfer state. J Phys Chem A;102:2555–2560.
31. Foster R., Kulevsky N., Wanigasekara D.S. (1974) Reaction of amino-acids with *p*-benzoquinones. J Chem Soc, Perkin Trans;1:1318–1321.
32. Adams R.D., Miao S. (2004) Metal carbonyl derivatives of 1,4-quinone and 1,4-hydroquinone. J Am Chem Soc;126:5056–5057.
33. Nakatsuji S.I., Nobusawa M., Suzuki H., Akutsu H., Yamada J.-I. (2009) Spin-carrying benzoquinone derivatives. J Org Chem;74:9345–9350.
34. Jia W.-G., Han Y.-F., Lin Y.-J., Weng L.-H., Jin G.-X. (2009) Stepwise formation of half-sandwich iridium-based rectangles containing 2,5-diarylamino-1,4-benzoquinone derivative linkers. Organometallics;28:3459–3464.
35. Gleeson B., Claffey J., Ertler D., Hogan M., Müller-Bunz H., Paradisi F., Wallis D., Tacke M. (2008) Novel organotin antibacterial and anticancer drugs. Polyhedron;27:3619–3624.
36. Benigni R. (2005) Structure-activity relationship studies of chemical mutagens and carcinogens: mechanistic investigations and prediction approaches. Chem Rev;105:1767–1800.
37. Qabaja G.M., Perchellet E., Perchellet J.-P., Jones G.B. (2000) Regioselective lactonization of naphthoquinones: synthesis and antitumoral activity of the WS-5995 antibiotics. Tetrahedron Lett;41:3007–3010.

Supporting Information

Additional Supporting Information may be found in the online version of this article:

Figure S1. ^{1}H NMR of compound **4**.

Figure S2. ^{13}C NMR of compound **4**.

Figure S3. ^{1}H NMR of compound **5**.

Figure S4. ^{13}C NMR of compound **5**.

Figure S5. ^{1}H NMR of compound **6**.

Figure S6. ^{13}C NMR of compound **6**.

Figure S7. ^{1}H NMR of compound **7**.

Figure S8. ^{13}C NMR of compound **7**.

Figure S9. ^{1}H NMR of compound **8**.

Figure S10. ^{13}C NMR of compound **8**.

Figure S11. ^{1}H NMR of compound **9**.

Figure S12. ^{13}C NMR of compound **9**.

Figure S13. Photograph of compounds 1–9 showing range of colours.

Table S1. Bond lengths [Å] and angles [°] for **1**.

Table S2. Bond lengths [Å] and angles [°] for **2**.

Table S3. Bond lengths [Å] and angles [°] for **3**.

Table S4. Bond lengths [Å] and angles [°] for **6**.

Table S5. Bond lengths [Å] and angles [°] for **9**.

Table S6. HRMS for compounds **3**, **4**, **7** and **8**.

Please note: Wiley-Blackwell is not responsible for the content or functionality of any supporting materials supplied by the authors. Any queries (other than missing material) should be directed to the corresponding author for the article.